

Gain measurements of scattering-assisted terahertz quantum cascade lasers

David Burghoff,^{1,a)} Chun Wang Ivan Chan,¹ Qing Hu,¹ and John L. Reno²

¹*Department of Electrical Engineering and Computer Science, Research Laboratory of Electronics, Massachusetts Institute of Technology, Cambridge, Massachusetts 02139, USA*

²*Center for Integrated Nanotechnologies, Sandia National Laboratories, Albuquerque, New Mexico 87123, USA*

(Received 20 March 2012; accepted 18 June 2012; published online 29 June 2012)

Using terahertz time-domain spectroscopy, the gain of scattering-assisted terahertz quantum cascade lasers is measured. By examining the intersubband gain and absorption over a wide range of bias voltages, we experimentally detect energy anticrossings—revealing information about the mechanism of laser action—and compare the resonant-tunneling injection scheme to the scattering-assisted injection scheme. The temperature performance of the gain medium is also measured and discussed, and an additional intersubband transition is identified that contributes to scattering-assisted lasing action at high temperatures. © 2012 American Institute of Physics.

[<http://dx.doi.org/10.1063/1.4732518>]

Terahertz quantum cascade lasers¹ (THz-QCLs) have matured greatly in recent years as compact semiconductor sources of terahertz radiation, but have unfortunately been limited to cryogenic operation thus far. Though recent work² has demonstrated operating temperatures as high as ~ 200 K, putting THz-QCLs close to the operating range of thermoelectric coolers, they still require cryogenic operation to obtain usable power levels. The traditional means of achieving high-temperature operation rely^{2,3} on the resonant-phonon injection scheme, in which electrons are injected into the upper lasing state by resonant tunneling and leave the lower lasing state through a combination of resonant extraction and emission of LO phonons. However, this mechanism is unsuitable for high-temperature operation of QCLs operating below 2 THz, since the dynamic range of an injection-based QCL is approximately proportional to its lasing frequency. To remedy this issue, THz QCLs have been recently developed that utilize scattering-assisted injection, in which electrons are injected into the upper state by the direct emission of a LO phonon.⁴⁻⁶ In particular, the gain medium demonstrated in Ref. 4 was able to achieve lasing at ~ 1.8 THz up to a temperature of 163 K, which is the highest operating temperature for a QCL operating below 2 THz to date. This gain medium also exhibited resonant-injection based lasing at ~ 4.0 THz up to a temperature of 151 K, making it potentially useful in broadband heterogeneous QCLs.^{7,8}

In order to better understand the operation of this device, it would be useful to investigate how its gain evolves with bias and temperature. To that end, we have used terahertz time-domain spectroscopy (THz-TDS) to perform transmission spectroscopy on such devices under bias, using a method similar to the integrated technique described in Ref. 9. Because terahertz pulses from external sources cannot be efficiently coupled into metal-metal waveguides, a second emitter section comprised of the laser ridge is instead used as a photoconductive switch, guaranteeing that the mode of the terahertz pulse matches the mode of the laser under test.^{9,10} However, in

contrast to previous studies, in which we have used an integrated emitter section, here we simply end-coupled two existing Fabry-Perot devices onto a single mount. The major advantage of this method is that it simplifies the necessary fabrication and allows for the efficient coupling of any two waveguides with the same dimensions, even ones produced from different gain media or ones produced by wet-etching. However, as the emitter section must be kept long enough to handle, the presence of an inert strongly coupled cavity can greatly increase the total optical losses for the laser. Although this prevents a loss measurement of the uncoupled cavity, lasing can be inhibited in such structures, allowing the measurement of unclamped gain and the properties of the gain medium alone.

The end-coupled devices used in the measurement were constructed by cleaving the wafer into two sections, aligning them using a micromanipulator, gluing the pieces together from the top, indium-soldering them to a copper mount, removing the glue, and affixing a silicon hyperhemispherical lens. The two sections can be accurately aligned to within ~ 1 μm of each other and are comparable in performance to integrated emitters. The devices tested were from the same gain medium as was described in Ref. 4, labeled OWI185E-M1 (wafer VB0244), and were wet-etched to keep the optical losses as low as possible. The data from two lasers will be presented here: Device A was 60- μm wide and 0.6-mm long, while device B was 40- μm wide and 1.05-mm long. Both devices were equipped with an emitter section approximately 0.5-mm long. In order to measure the gain of each device, near-infrared pulses from a Ti:Sapphire (with a 70 fs pulse width, 785 nm center wavelength, and 100 mW power) were focused onto the emitter sections, which were biased at -20 V with a 120 kHz square wave. The laser sections themselves were biased at 10% duty cycle and were triggered off of every other emitter bias pulse, so that signals obtained when the laser was on and when it was off could be compared. Electro-optic sampling¹¹ was performed using a 300- μm GaP crystal, and a pair of lock-in amplifiers tuned to 60 kHz and 120 kHz were used to detect the terahertz field transmitted through the device. These

^{a)}Electronic mail: burghoff@mit.edu.

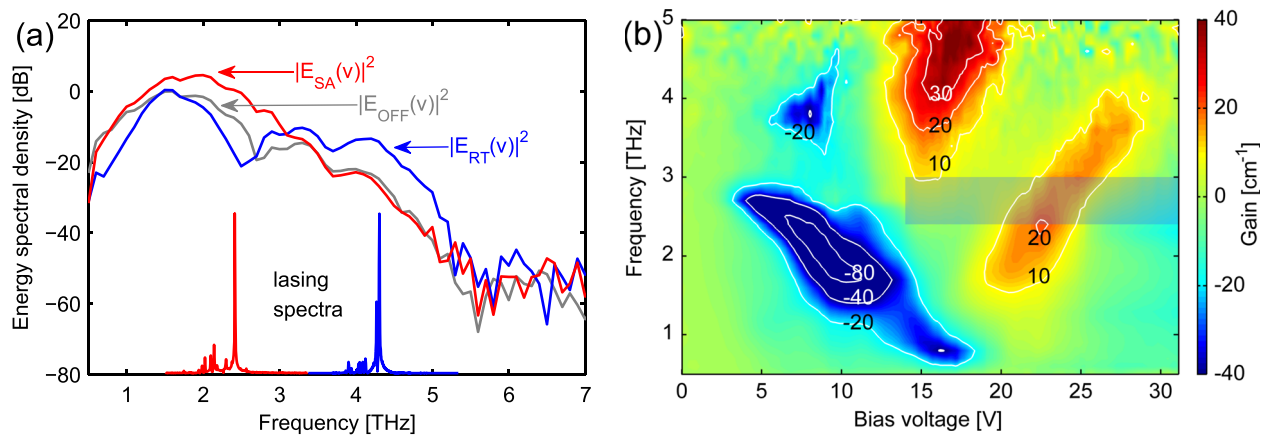


FIG. 1. (a) Sample TDS spectra taken from device B, showing spectra obtained with no bias (grey), high-frequency lasing (blue), and low-frequency lasing (red). Lasing spectra at 35 K are also shown for reference. (b) Contour plot showing the measured gain/absorption of device A at 35 K versus frequency and bias voltage. The shaded region indicates the region where the absorption artifact was removed.

signals are processed to determine the field transmitted with the laser on and with the laser off (e.g., see Ref. 12).

Figure 1(a) shows the frequency content associated with pulses transmitted through device B at 35 K. When the laser is off, the transmitted pulse has a slow-varying frequency response, with the exception of an absorption feature at 2.7 THz. This feature corresponds to absorption from the first excited state of the unbiased module to the second and has an oscillator strength of about 0.7. This feature is relatively unimportant since it vanishes under design bias, but matters insofar as the gain of the QCL is always measured with respect to the gain at zero bias. Since a reduction in losses is indistinguishable from an increase in gain, all measurements at much higher biases will therefore show a “gain” that peaks at 2.7 THz, which is actually an artifact from the vanishing absorption. Fortunately, its linewidth is relatively narrow (~ 0.5 THz), and it is located away from the peak lasing frequencies. When the device is biased to be lasing in the resonant-tunneling and scattering-assisted regimes, peaks in the transmitted spectra appear at around ~ 4 THz and around ~ 2 THz, respectively, corresponding to the presence of both types of gain. Note that the bandwidth of the generated terahertz pulse is quite high—above 5 THz—enabling THz-TDS measurements on most QCLs operating below the Reststrahlen band of GaAs.

Figure 1(b) shows a contour plot of the results of a gain measurement of device A at 35 K. Since device A’s emitter section was nearly as long as its laser section, its overall cavity losses were effectively doubled, and the device no longer lases, even at low temperatures. Therefore, Fig. 1(b) is a measure of the gain medium’s properties without the influence of optical feedback. The I-V characteristics of this device are not shown and are similar to the I-V characteristics of the non-lasing device described in Ref. 4; its major distinctive feature is the lack of any obvious negative differential resistance (NDR). Finally, we note that the aforementioned absorption artifact at 2.7 THz was digitally removed by interpolating between the closest frequencies unaffected by it; this region is shaded to indicate the region in which data were altered.

Figure 2(a) shows the same data alongside the frequency of the relevant transitions determined by band structure

simulations (whose wavefunctions are shown in Figure 2(b)). For ease of interpretation, we use two naming schemes to track their energies: low-bias wavefunctions are denoted by letters and are labeled according to their zero bias counterparts, while high-bias wavefunctions are denoted by numbers and are labeled according to their design bias counterparts. At low biases, there is a regime in which strong absorption can be observed, absorption that appears to be dominated by the $b \rightarrow c$ transition. However, a closer examination reveals that there are at least two features superimposed on each other, each of which contribute to the total absorption. This could be seen directly from the anticrossings observed in Fig. 2(a), but is made much clearer by Fig. 2(c), which shows the low-frequency characteristics of the design at several bias points in the regime in which resonant tunneling injection lasing occurs. At 13.7 V, the absorption profile is asymmetric because it is comprised of multiple superimposed peaks, but they are not resolvable. At 16.2 V, their separation is increased and they are more distinguishable, showing one at ~ 0.8 THz and another at ~ 1.4 THz. By 18.6 V, the higher-frequency transition has started experiencing positive net gain, while the lower-frequency transition remains lossy. Each feature red-shifts to a minimum value before blue-shifting, strongly indicating that the observed behavior corresponds to anticrossings in progress. From band structure simulations, we identify the lower-frequency absorption as occurring between states 1 and 2, while the higher-frequency transition occurs mainly between states 5 and 4, the scattering-assisted lasing transition. It is also possible that the $4 \rightarrow 3$ transition provides some gain at this temperature, but we expect it to be weaker than the $5 \rightarrow 4$ transition thanks to its reduced upper state lifetime ($\tau_4(1 - \tau_3/\tau_{43}) = 1.41$ ps, compared with $\tau_5(1 - \tau_4/\tau_{54}) = 2.70$ ps) and its broader linewidth (estimated to be $\Delta\nu_{43} = 1.47$ THz, compared with $\Delta\nu_{54} = 0.98$ THz).

It is also worth comparing the dynamic range and frequency coverage of the resonant-tunneling injection (RT) and scattering-assisted injection (SA) transitions, as they have some interesting differences arising from their different modes of operation. RT lasing occurs between states 1’ and 5, peaking at about 16 V, while SA lasing occurs between states 5 and 4, peaking at about 22 V. Though the RT

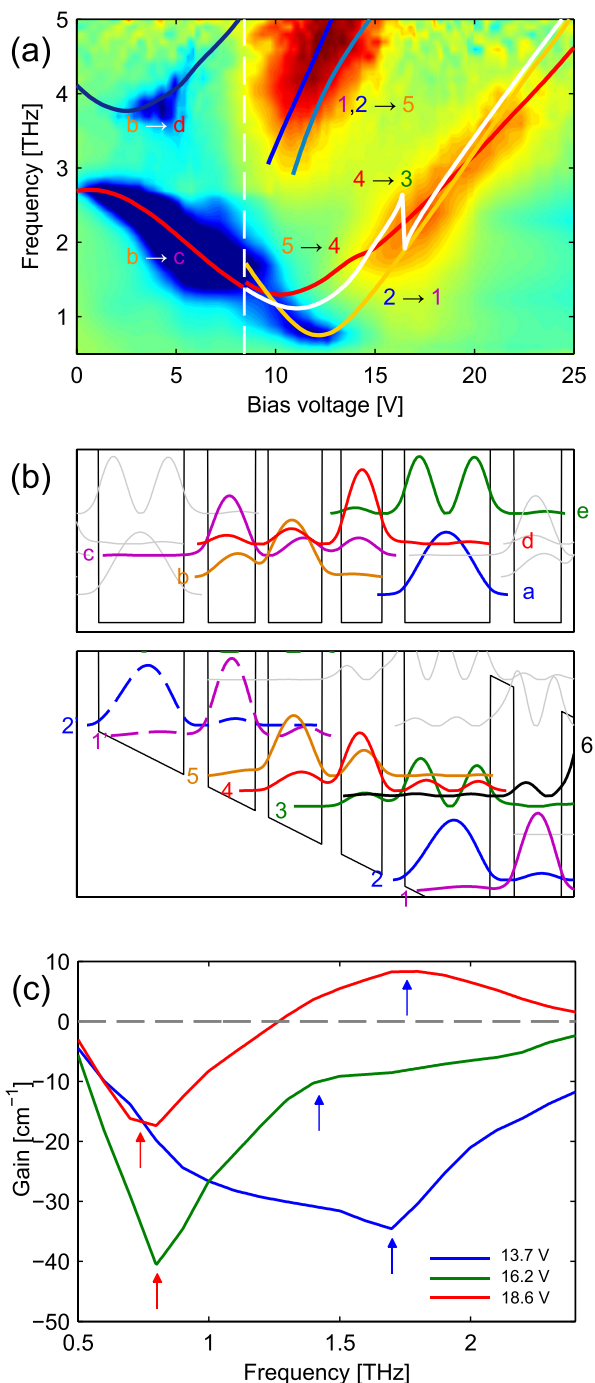


FIG. 2. (a) Simulated transition energies with gain data. Transitions to the left of the white dotted line are labeled according to the zero-bias wavefunctions (letters), while transitions to the right are labeled according to design-bias wavefunctions (numbers). The true voltage across the QCL is determined assuming a Schottky contact drop of 3 V and a series resistance of 4 Ω . (b) Band diagram of the scattering-assisted gain medium at zero bias (0 V) and at design bias (15 V). Scattering-assisted lasing occurs between levels 5 and 4; resonant-tunneling lasing occurs between levels 1' and 5. (c) Measured low frequency gain/absorption at several points near the resonant-tunneling injection design bias, showing the evolution of the two peaks.

transition has a much higher peak gain at this temperature, its dynamic range is considerably smaller. Referring to Fig. 1(b), if we define dynamic range as the range over which the gain exceeds 10 cm^{-1} , the RT transition has a dynamic range of 7 V while the SA transition has a dynamic range of nearly 10 V. This is a result of the fact that the SA injection

mechanism is only weakly dependent on subband alignments and can occur provided that the separation between the injector and upper lasing state is near the LO phonon separation (36 meV in GaAs). In contrast, the RT injection mechanism depends on the injector and upper lasing state being precisely aligned to achieve efficient resonant tunneling. Of course, the large dynamic range also leads the SA transition to have broad frequency coverage, experiencing substantial gain at frequencies as low as 1.5 THz (at 17 V) and as high as 4.0 THz (at 27 V). In principle, this type of gain medium could be extremely useful for applications that require frequency-agile broadband sources, such as swept-source OCT.¹³

To glean more information about this design, we have also examined the temperature dependence of its gain. Device B was tested at temperatures ranging from 35 K to 200 K (well beyond the point at which both transitions stop lasing), and Figure 3(a) shows the resulting gain at the two main frequencies of interest and at fixed bias. First, consider the RT transition, shown in blue. Because the emitter section of device B is only half the length of the laser section, this device actually lased in the RT mode at temperatures below 90 K. Therefore, gain clamping is observed at $\sim 24 \text{ cm}^{-1}$, a value that is approximately 50% larger than the losses expected from an uncoupled laser. This can be confirmed by considering the gain for the RT injection at $T_{\text{max}} = 151 \text{ K}$, $\sim 17 \text{ cm}^{-1}$, which in an uncoupled cavity would be the threshold gain. The SA transition is shown in red and shows a very distinct non-monotonic behavior: as temperature is increased, its gain increases, reaching a peak value at 110 K before it begins to decay. However, this result was somewhat unexpected since the peak light output observed from a device lasing in the SA mode actually decays monotonically with increasing temperature. We argue that this discrepancy is actually due to the spectral shift of the low-frequency lasing: at low temperatures, the low-frequency lasing occurs at frequencies as high as 2.4 THz, but at high temperatures, it occurs only at 1.8 THz. Though the gain at 1.8 THz may increase, the peak optical power is determined by the gain at higher frequencies, which does decrease monotonically. The 1.8 THz gain only becomes relevant once the higher frequency components have completely subsided; for most devices, this occurs at temperatures above 100 K.

In principle, this effect could be investigated by simply plotting the gain spectra at elevated temperatures, but in practice, this is difficult since the artifact at 2.7 THz merges with the SA peak at high temperatures for frequencies above 2 THz, as the b→c transition is thermally activated and affects a larger frequency range due to its increased magnitude. It may be tempting to argue that the increase in gain with temperature at 1.8 THz is a result of similar artifact, but there are several reasons why this cannot be the case, chief of which is the fact that the measured gain at the SA T_{max} (163 K) is 19 cm^{-1} , a value which is close to the waveguide losses of 18 cm^{-1} measured in other devices with similar waveguides.⁹ If flat-band absorption at $\sim 2.7 \text{ THz}$ was significantly boosting the gain normalized to this absorption, then this value (19 cm^{-1}) would be artificially boosted. Moreover, a hallmark of such behavior is that the measured gain would not return to zero far past the design bias, but this is not the case (see Fig. 1(b)).

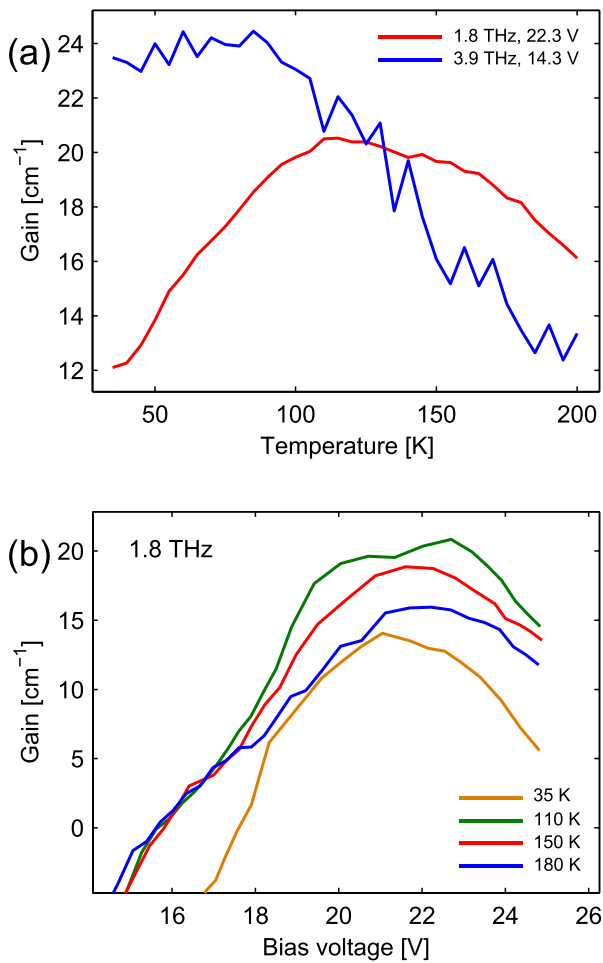


FIG. 3. (a) Temperature dependence of the gain of device B, at fixed frequency and fixed bias. The bias values are chosen to fall in the corresponding lasing regime. (b) Gain of device A at 1.8 THz, at 35 K, 110 K, 150 K and 185 K, versus bias voltage.

In order to explain the origin of the spectral shift, we plot in Fig. 3(b) the 1.8 THz gain of device A at 35 K, 110 K, 150 K, and 180 K, swept across the SA design bias range. The peak gain at 110 K is the highest of the four curves shown and also shows two peaks, one at 20.7 V and at 22.7 V. At higher temperatures, only one peak is clearly resolved, and the voltage at which the peak gain is observed shows a slight upward shift. Since the subband alignments in the system should be relatively independent of temperature (for constant voltage), this suggests that there are multiple transitions contributing to the total gain of the SA transition at elevated temperatures. Therefore, we argue that there is an additional contribution to the gain arising from the $2' \rightarrow 1'$ transition. This contribution is of lower frequency than the $5 \rightarrow 4$ transition, and reaches 1.8 THz at a higher bias, when $E_{1'5}$ approaches 36 meV and state $1'$ is efficiently depopulated by LO phonons. This explains the dual-peaked behavior of moderate temperatures: both transitions contribute to gain at 1.8 THz, but do so at different biases. This interpretation also

explains the peculiar non-monotonic behavior seen at 1.8 THz, since the depopulation of state $1'$ becomes more efficient at elevated temperatures due to increased LO phonon emission, which of course comes at the expense of gain in the RT lasing mode. Because the linewidths at high temperatures are fairly broad, both transitions can contribute to the total lasing action near T_{\max} , although the $5 \rightarrow 4$ transition is less effective.

In conclusion, we have used terahertz time-domain spectroscopy to characterize the performance of scattering-assisted THz-QCL gain media. From these measurements, we were able to examine the behavior of absorption features related to energy anticrossings in the system and were able to observe several important differences between the resonant-tunneling and scattering-assisted lasing schemes. We also examined the temperature performance of this structure and used this information to identify a third transition contributing to the laser's performance at high temperatures.

The work at MIT is supported by NASA and NSF. This work was performed, in part, at the Center for Integrated Nanotechnologies, a U.S. Department of Energy, Office of Basic Energy Sciences user facility. Sandia National Laboratories is a multi-program laboratory managed and operated by Sandia Corporation, a wholly owned subsidiary of Lockheed Martin Corporation, for the U.S. Department of Energy's National Nuclear Security Administration under Contract No. DE-AC04-94AL85000. The authors would also like to thank Sushil Kumar for his fabrication of the wafers used in this project.

- ¹R. Kohler, A. Tredicucci, F. Beltram, H. E. Beere, E. H. Linfield, A. G. Davies, D. A. Ritchie, R. C. Iotti, and F. Rossi, *Nature (London)* **417**, 156–159 (2002).
- ²S. Fatholouloumi, E. Dupont, C. Chan, Z. Wasilewski, S. Laframboise, D. Ban, A. Mátyás, C. Jirauschek, Q. Hu, and H. Liu, *Opt. Express* **20**, 3866–3876 (2012).
- ³S. Kumar, Q. Hu, and J. L. Reno, *Appl. Phys. Lett.* **94**, 131105 (2009).
- ⁴S. Kumar, C. W. I. Chan, Q. Hu, and J. L. Reno, *Nat. Phys.* **7**, 166–171 (2011).
- ⁵M. Yamanishi, K. Fujita, N. Yu, T. Edamura, K. Tanaka, and F. Capasso, in *CLEO:2011—Laser Applications to Photonic Applications* (Optical Society of America, 2011), p. CMF1.
- ⁶E. Dupont, S. Fatholouloumi, Z. R. Wasilewski, G. Aers, S. R. Laframboise, M. Lindskog, S. G. Razavipour, A. Wacker, D. Ban, and H. C. Liu, *J. Appl. Phys.* **111**, 073111 (2012).
- ⁷D. Turčinková, G. Scalari, F. Castellano, M. I. Amanti, M. Beck, and J. Faist, *Appl. Phys. Lett.* **99**, 191104 (2011).
- ⁸J. R. Freeman, A. Brewer, J. Madéo, P. Cavalieri, S. S. Dhillon, J. Tignon, H. E. Beere, and D. A. Ritchie, *Appl. Phys. Lett.* **99**, 241108 (2011).
- ⁹D. Burghoff, T.-Y. Kao, D. Ban, A. W. M. Lee, Q. Hu, and J. Reno, *Appl. Phys. Lett.* **98**, 061112 (2011).
- ¹⁰M. Martl, J. Daro, C. Deutsch, M. Brandstetter, A. M. Andrews, P. Klang, G. Strasser, and K. Unterrainer, *Opt. Express* **19**, 733–738 (2011).
- ¹¹Q. Wu and X.-C. Zhang, *Appl. Phys. Lett.* **67**, 3523–3525 (1995).
- ¹²N. Jukam, S. Dhillon, Z.-Y. Zhao, G. Duerr, J. Armijo, N. Sirmons, S. Hameau, S. Barbieri, P. Filloux, C. Sirtori, X. Marcadet, and J. Tignon, *IEEE J. Sel. Top. Quantum Electron.* **14**, 436–442 (2008).
- ¹³A. W. M. Lee, T.-Y. Kao, D. Burghoff, Q. Hu, and J. L. Reno, *Opt. Lett.* **37**, 217–219 (2012).